Journal of The Electrochemical Society, **151** (3) F45-F53 (2004)
0013-4651/2004/151(3)/F45/9/$7.00 © The Electrochemical Society, Inc.

Organosilicate Spin-On Glasses

II. Effect of Physical Modification on Mechanical Properties

Yvete Toivola,[a] Suhan Kim,[b] Robert F. Cook,[a,z] Kookheon Char,[b] Jin-Kyu Lee,[c] Do Y. Yoon,[c] Hee-Woo Rhee,[d,*] Sang Youl Kim,[e] and Moon Young Jin[f]

[a]*Department of Chemical Engineering and Materials Science, University of Minnesota, Minneapolis, Minnesota 55455 USA*
[b]*School of Chemical Engineering and* [c]*School of Chemistry, Seoul National University, Seoul, Korea*
[d]*Department of Chemical Engineering, Sogang University, Seoul, Korea*
[e]*Advanced Materials Division, Korea Research Institute of Chemical Technology, Taejon 305-600, Korea*
[f]*Department of Chemistry, Korea Advanced Institute of Science and Technology, Daejon 305-701, Korea*

Porous copolymer films were synthesized from a methylsilsequioxane:1,2-bis(trimethoxysilyl)ethane (MSSQ:BTMSE) matrix and either an aromatic-core or aliphatic-core porogen at 10, 20, or 30 wt % porogen loading. Films were characterized using scanning electron microscopy (SEM), IR spectroscopy, and ellipsometry. Depth-sensing indentation experiments were performed to measure apparent film modulus, E_f', and hardness, H. Indentation load-displacement traces and SEM images were used to determine the threshold load for cracking, P_c. The aliphatic-core porogen produced a greater porosity film than the aromatic-core porogen for 10 wt % loading and smaller porosity films for 20 and 30 wt % loadings. IR spectra, normalized for film thickness and density, indicated decreased O-Si-O networking in porous MSSQ:BTMSE films. The combination of increased porosity and decreased O-Si-O networking led to a decreased apparent E_f' and H relative to the unmodified MSSQ:BTMSE film. However, low-porosity (approximately 7%), aliphatic-porogen MSSQ:BTMSE films are optimized relative to unmodified MSSQ with smaller dielectric constant and greater E_f' and H.
© 2004 The Electrochemical Society. [DOI: 10.1149/1.1643073] All rights reserved.

Manuscript submitted April 7, 2003; revised manuscript received September 11, 2003. Available electronically January 26, 2004.

In order to maintain current microelectronic device performance while scaling down feature dimensions in the interconnection array, low-dielectric-constant, low-k, materials are needed to replace SiO_2 ($k \approx 4$). Industry goals require $k < 2.4$ (for a pitch of 210 nm) by the year 2004 and further decreases to $k < 2$ by year 2010 (for a pitch of 105 nm).[1] It is expected that such decreases in dielectric constant will be realized by reductions in material density through incorporation of porosity.[2]

Porous silicate ($1.02 < k < 3$),[3-6] organic ($1.65 < k < 2.7$),[7-9] and organosilicate ($1.5 < k < 2.7$)[10-16] based low-k dielectric films have been synthesized to meet these goals. One common synthesis procedure uses two immiscible materials, a thermally stable material that acts as the host (matrix) for a thermally labile, pore-generating (porogen) material.[17] During an initial heating stage, the porogen phase segregates within the matrix to form small (nanoscopic) domains. On heating to higher temperatures the porogen thermally decomposes and diffuses through the matrix,[18] leaving voids corresponding to the original phase-segregated morphology.[2]

While k may be reduced by decreasing material density, the reductions are achieved at the expense of film mechanical integrity. Successful integration of any dielectric material requires adequate film properties of modulus, hardness, toughness, and adhesion[19] to maintain device integrity through routine fabrication procedures such as chemical mechanical polishing (CMP)[20-22] and packaging,[23] which involve severe mechanical loading. Modulus and hardness are reduced with increased porosity as the pores disrupt the material connectivity. Adhesion is also degraded with increased porosity as there is less surface area available for bonding to a neighboring material. It seems that maintaining mechanical integrity while decreasing k solely via increased porosity is unlikely to produce a material suitable for integration.

However, k scales not only with material density but also with the polarizability of the matrix material. Therefore, k may be reduced by using a matrix of smaller polarizability than that of SiO_2[2] and a balance between desired decreases in k while maintaining adequate mechanical integrity realized by incorporating a small amount of porosity in an already low-k matrix material.

The primary focus of this paper is the mechanical properties of porous methylsilsesquioxane (MSSQ):1,2-bis(trimethoxysilyl)ethane (BTMSE) copolymer films. MSSQ ($MeSiO_{3/2}$) is a promising candidate SiO_2 replacement material with a dielectric constant of 2.7[24] that retains the O-Si-O backbone of SiO_2, allowing for the possibility of optimizing modulus, hardness, and toughness along with dielectric constant.[25] Previous studies have shown the feasibility of synthesizing porous MSSQ-based materials to achieve decreased dielectric constants with increased porosity.[10-14] However, the key to engineering a porous film with adequate mechanical properties lies in the integrity of the matrix material, and MSSQ:BTMSE copolymer films have been shown in a previous study[26] to have approximately doubled modulus, E', hard-

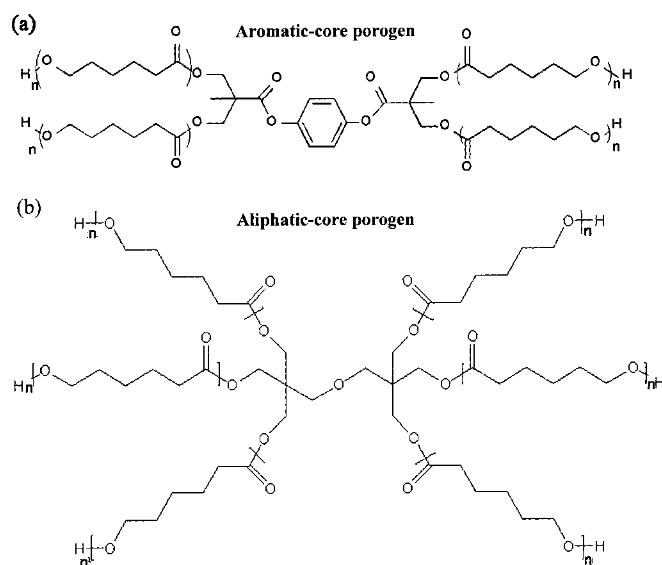

Figure 1. Two-dimensional figures show the (a) four-arm aromatic and (b) six-arm aliphatic pore-generating (porogen) molecules.

* Electrochemical Society Active Member.
[z] E-mail: rfc@cems.umn.edu

Downloaded 20 Jul 2009 to 147.46.182.29. Redistribution subject to ECS license or copyright; see http://www.ecsdl.org/terms_use.jsp

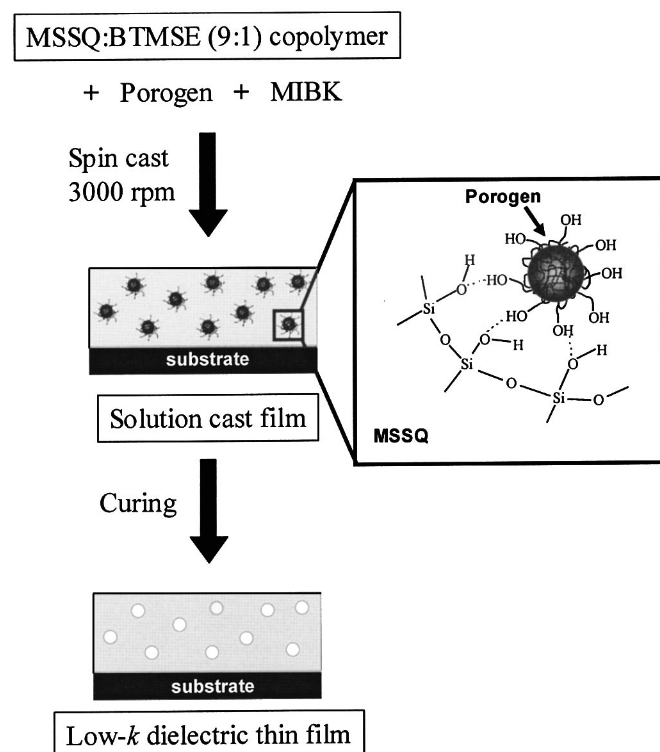

Figure 2. A schematic flowchart illustrates the procedure used to create porous films. A porogen is added to the MSSQ:BTMSE copolymer film prior to spin casting. The hydrophobic porogen core phase-segregates from the copolymer matrix, leaving pores behind after calcination.

ness, H, and crack threshold load, P_c, than base MSSQ. The enhancement in mechanical properties came at the expense of only a slight increase in dielectric constant from 2.70 to 2.86 relative to MSSQ. An anticipated result is that using MSSQ:BTMSE as the matrix material will provide the basis for improved mechanical properties of porous MSSQ:BTMSE films relative to porous MSSQ films.

Two types of sacrificial polymers were used in this study and are shown in Fig. 1, where (a) is a four-armed aromatic-core porogen and (b) is a six-armed aliphatic-core porogen. The porogens were added in different amounts (10, 20, or 30 wt %) to the base MSSQ:BTMSE material. The mechanical properties of porous copolymer films were measured and compared to unmodified MSSQ and MSSQ:BTMSE films.

Experimental

Material synthesis and film processing.—A copolymer film was prepared by the polymerization of 90 mol % methyltrimethoxysilane (MTMS) and 10 mol % 1,2-bis(trimethoxysilyl)ethane (BTMSE) monomers. The synthesis of the MSSQ:BTMSE (9:1) copolymer was similar to the procedure described in Ref. 27. The two star-shaped polymers shown in Fig. 1 were used as sacrificial pore-generating (porogen) materials, with average degrees of polymerization of each arm, N, and molecular weights of (a) the aliphatic-core porogen, $N = 5.5$ and $\bar{M}_n = 4420$ g mol^{-1} ($\bar{M}_w = 5210$ g mol^{-1}), and (b) the aromatic-core porogen, $N = 7.5$ and $\bar{M}_n = 3940$ g mol^{-1} ($\bar{M}_w = 4186$ g mol^{-1}).

Silicon (100) wafers were cut into 1 × 1 cm pieces and cleaned with a piranha solution (H_2SO_4 and H_2O_2, volume ratio of 3:1) to remove organic contaminants, followed by a deionized water rinse, then dried under a nitrogen stream. Figure 2 is a schematic diagram showing the processing procedure used to prepare the porous films. The MSSQ:BTMSE copolymer precursor was mixed with 10, 20, or 30 wt % porogen, and solutions of 20 wt % solids in methyl isobutyl ketone (MIBK) were made. Solutions were deposited on silicon pieces through a syringe with a 0.2 μm polytetrafluoroethane (PTFE) filter and spun at 3000 rpm for 30 s. On deposition, the hydrophobic porogen core formed small domains within the hydrolyzed MSSQ:BTMSE matrix while pendant hydroxyl groups formed hydrogen bonds with the matrix, as highlighted in the inset in Fig. 2. Films were cured under nitrogen with a curing cycle of heating at 3°C/min to 250°C, held at temperature for 30 min, heated at 3°C/min to 420°C, and held at temperature for 40 min, before slow cooling.

On initial heating the matrix and porogen phase separate until, at about 250°C, the matrix begins to vitrify. On continued heating the matrix exhibits sufficient stiffness such that during the holding temperature of 420°C the decomposition of the porogen occurs without pore collapse. (Pore collapse was inferred from refractive index measurements for loading >40 wt % for the aromatic-core porogen, but no pore collapse was observed for the aliphatic-core porogen.) The degradation temperature of the porogen can thus be controlled by changing the arm chain structure and end functional groups without interfering with the vitrification-condensation reaction of the matrix. An idealized schematic diagram of the final porous MSSQ:BTMSE film is shown in Fig. 2.

Structural and mechanical characterization.—Scanning electron microscopy (SEM) images of fracture cross sections were used to measure film thickness, t_f, and to examine the texture of the porous films (SEM, JEOL 6500). SEM was also used to image permanent deformation from indentation experiments. Film thickness, t_f, is listed in Table I for all films.

Depth-sensing indentation (DSI) experiments were performed using a commercial indenter to evaluate the mechanical properties of all films (Nano Indenter® XP, MTS Corp.). A diamond Berkovich (three-sided pyramid) indentation tip was used to perform eight indentations at each peak load for all samples. Load-displacement (P-h) traces were used to quantify the relative energy dissipated during contact,[26] $D_{P\text{-}h}$, and the threshold load for cracking, P_c.[28] Apparent plane strain modulus, E', and hardness, H, were calculated as a function of displacement during each indentation using continuous stiffness measurement (CSM).[29] Average values of E'

Table I. Film thickness, t_f, refractive index, n, and volume percent porosity for porous MSSQ:BTMSE films.

	Aromatic-core porogen			Aliphatic-core porogen			
Porogen loading (wt %)	Film thickness, t_f (nm)	Refractive index, n	Volume fraction porosity, ϕ	Film thickness, t_f (nm)	Refractive index, n	Volume fraction porosity, ϕ	Dielectric constant, k
0	776	1.389	0	776	1.389	0	2.86
10	767	1.365	0.055	827	1.358	0.072	2.63
20	670	1.323	0.154	784	1.338	0.118	2.42
30	686	1.128	0.268	743	1.295	0.221	2.21

Downloaded 20 Jul 2009 to 147.46.182.29. Redistribution subject to ECS license or copyright; see http://www.ecsdl.org/terms_use.jsp

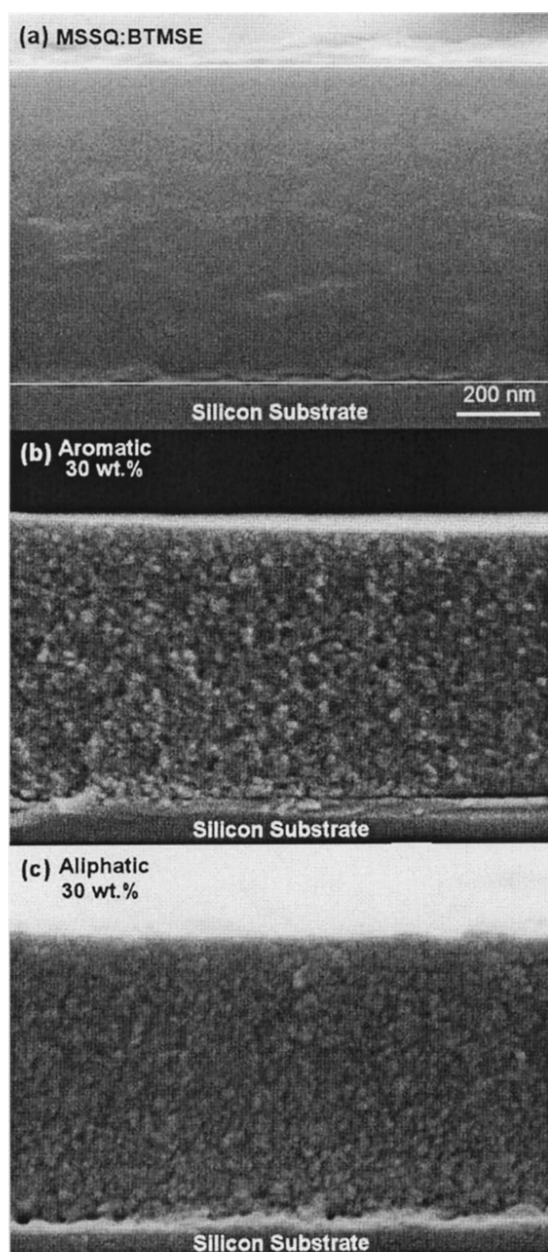

Figure 3. SEM images of films in cross section for (a) unmodified and porous MSSQ:BTMSE films with 30 wt % loading of the (b) aromatic-core porogen or (c) aliphatic-core porogen. While the unmodified film appeared smooth, porous films showed obvious film texture likely arising from porosity.

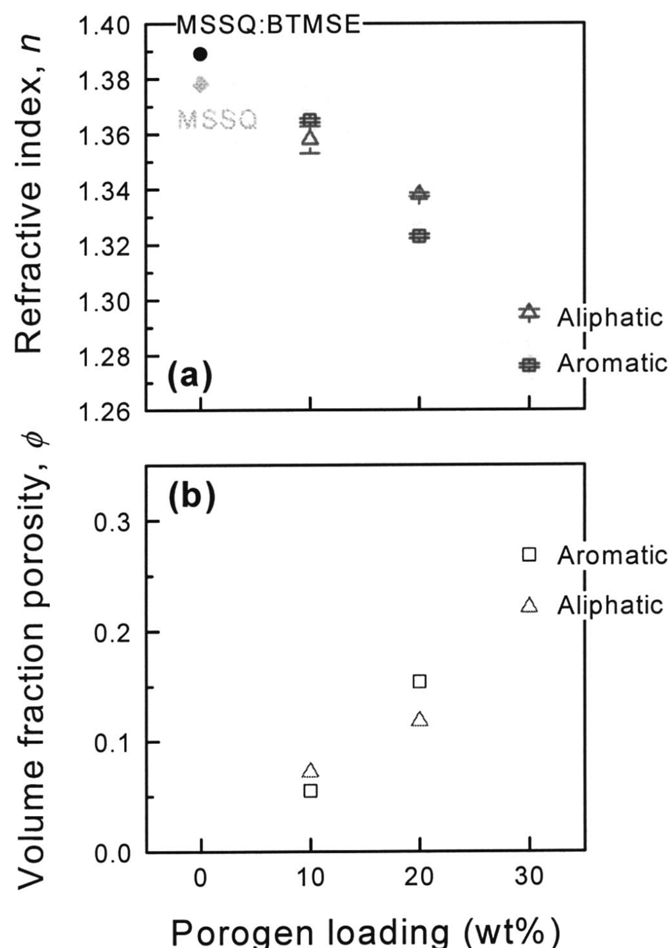

Figure 4. (a) A plot of the measured refractive index, n, as a function of wt % porogen loading for porous MSSQ:BTMSE films relative to unmodified MSSQ:BTMSE and MSSQ films shows decreased refractive index with increased porogen loading. (b) A plot of the calculated volume fraction porosity, ϕ, as a function of wt % porogen loading shows how porosity increased with increased porogen loading.

and H were determined every 5 nm in displacement, h, over a peak indentation load, P_{max}, ranging from 0.1 to 300 mN.

Optical and dielectric characterization.—The refractive index, n, of unmodified and porous MSSQ:BTMSE copolymer films was determined from ellipsometry experiments (L116B-85B, Gaertner sci). Refractive index, n, is listed in Table I for all films. Dielectric constant, k, measurements were made with metal-insulator-semiconductor (MIS) structures for films fabricated with the aliphatic-core porogen, and relative dielectric constant values are listed in Table I. As expected, k decreased from the base value of 2.86 to 2.21 with increased porogen loading.

Fourier transform infrared (FTIR) spectroscopy was performed in transmission mode over the frequency range 400-4000 cm^{-1} with 4 cm^{-1} spectral resolution (Nicolet Series II Magna-IR System 750). Spectra were analyzed to determine changes in bonding as a function of porosity for all films.

Results

Figure 3 shows three SEM images of cross-sectioned MSSQ:BTMSE films on silicon substrates. Figure 3a is an unmodified MSSQ:BTMSE film, (b) is a film with 30 wt % loading of the aromatic-core porogen, and (c) is a film with 30 wt % loading of the aliphatic-core porogen. The fracture surface of the unmodified MSSQ:BTMSE film appeared smooth while those of the porous films were textured, reflecting the latter films' porosity. The surface texture of the film made with the aliphatic-core porogen appeared finer than that of the film made with the aromatic-core porogen for the same weight percent loading.

Figure 4a is a plot of the measured refractive index, n, as a function of porogen loading for aliphatic and aromatic porogen-modified films. The refractive indexes of unmodified MSSQ and MSSQ:BTMSE films are shown for reference. Although the MSSQ:BTMSE copolymer film had a larger refractive index than MSSQ, all porous copolymer films had refractive indexes less than that of MSSQ and exhibited decreases with increased porogen loading that depended on the porogen used. (Similar remarks can be made regarding dielectric constant. All aliphatic-core porogen copolymer materials exhibited dielectric constants less than that of

Downloaded 20 Jul 2009 to 147.46.182.29. Redistribution subject to ECS license or copyright; see http://www.ecsdl.org/terms_use.jsp

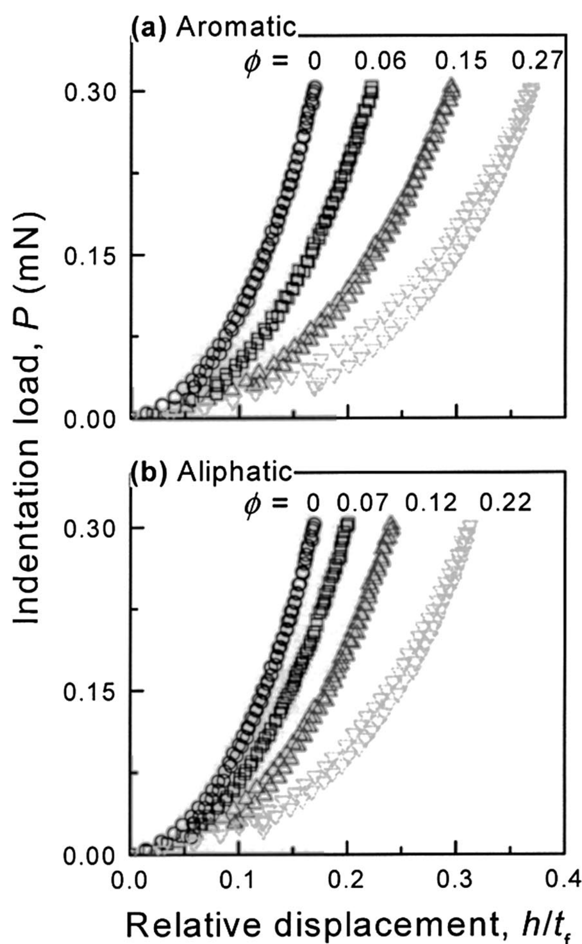

Figure 5. Indentation load-displacement traces for 0.3 mN peak load indentations in porous and unmodified MSSQ:BTMSE films where displacement was normalized by film thickness, t_f. Two plots show the P-(h/t_f) indentation response for films made with (a) the aromatic-core porogen and (b) the aliphatic-core porogen relative to unmodified MSSQ:BTMSE. Film porosity, ϕ, listed above the indentation trace illustrates that the relative displacement at peak load, $h(P_{max})/t_f$, increased with increased porosity.

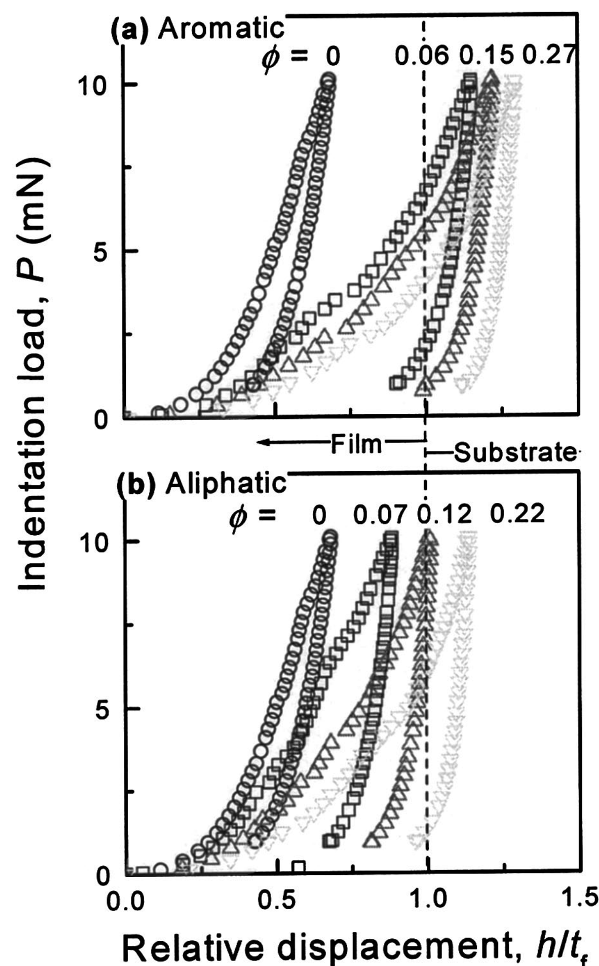

Figure 6. Indentation P-(h/t_f) traces for 10 mN peak load indentations in unmodified and porous MSSQ:BTMSE films where the dashed vertical line indicates the film-substrate interface. Traces for films made with the (a) aromatic-core porogen and (b) the aliphatic-core porogen are shown relative to unmodified MSSQ:BTMSE. For each porogen type, the relative displacement at peak load, $h(P_{max})/t_f$, increased with increased porosity.

MSSQ and which further decreased with increased porogen loading.)

Refractive index is expected to scale with material density for these porous films, as all films were made with a MSSQ:BTMSE matrix. The index of refraction can thus be used to determine the volume fraction porosity, ϕ, of the porous MSSQ:BTMSE films using a Lorentz-Lorenz relation

$$\frac{n^2 - 1}{n^2 + 2} = (1 - \phi)\frac{n_0^2 - 1}{n_0^2 + 2}$$

where n_0 is the measured refractive index of the unmodified MSSQ:BTMSE matrix, and n is the measured refractive index of the porous MSSQ:BTMSE film. The calculated volume fraction porosity, ϕ, for each film is listed in Table I, noting that the unmodified base MSSQ:BTMSE reference film may itself be slightly porous (on a much finer scale than that induced by the incorporation of porogen). (Calculations using relative dielectric constant, k, in place of n^2 in the equation yield similar ϕ values for the aliphatic-porogen material.)

Figure 4b shows the inferred porosity, ϕ, *vs.* weight percent porogen loading for all MSSQ:BTMSE films. The volume fraction porosity increased with increased porogen loading as anticipated, and the rate of increase was different for the two porogens. As weight percent porogen loading is a processing parameter, film porosity, ϕ, a quantity describing the microstructure, is used to compare films for the remainder of this paper.

Figure 5 contains indentation traces and is a plot of load, P, as a function of relative displacement, h/t_f, for 0.3 mN peak load indentations in (a) aromatic-core porogen and (b) aliphatic-core porogen films relative to the unmodified MSSQ:BTMSE film. For this small indentation load, relative peak displacements were shallow, ranging from 10 to 35% of the film thickness. For the greatest porosity films for which $h(P_{max})/t_f > 0.2$, it is likely that the indentation response was influenced by the underlying stiff silicon substrate,[29] resulting in an increased stiffness of the observed indentation response. However, as the largest relative displacement at peak load was less than 50% of the film thickness, relative comparisons between films can be made using these traces.

Indentation responses were almost completely elastic for films with $\phi \leq 0.15$, and an increased degree of hysteresis for films was observed for films with $\phi \geq 0.22$. The unmodified MSSQ:BTMSE film showed the smallest h/t_f at peak load of all films; the systematic trend of increased relative peak displacement with increased porosity is evident in Fig. 5, almost regardless of the porogen type.

Figure 6 shows that for a peak indentation load of 10 mN, the relative displacement at peak load extended to, or penetrated, the film-substrate interface ($h/t_f = 1$, marked by a vertical dashed line).

Downloaded 20 Jul 2009 to 147.46.182.29. Redistribution subject to ECS license or copyright; see http://www.ecsdl.org/terms_use.jsp

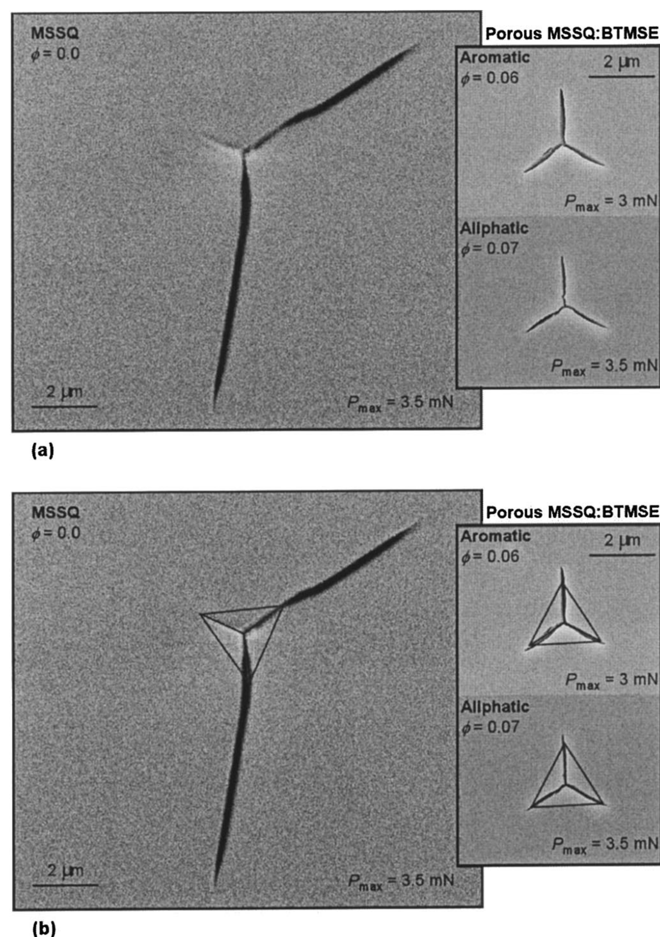

Figure 7. SEM images from peak indentation loads just greater than the crack-threshold load, P_c, show (a) residual indentation damage in the lowest porosity MSSQ:BTMSE films relative to the unmodified MSSQ film. (b) The effective contact area at peak load is drawn over each image to highlight film cracks extending past the indentation tip.

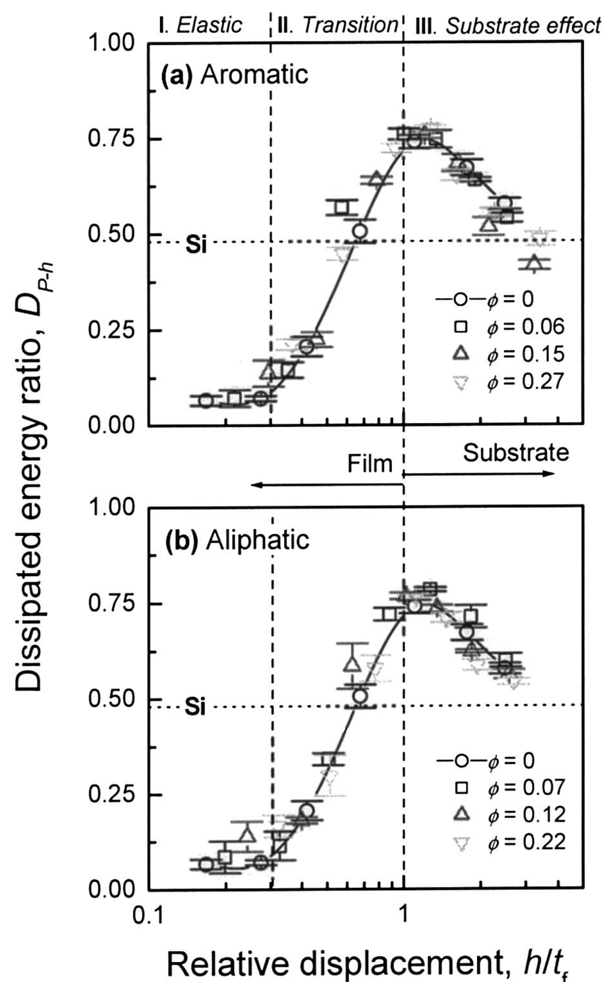

Figure 8. The dissipated energy ratio, $D_{P\text{-}h}$, for porous films made with (a) aromatic and (b) aliphatic core porogen (symbols) relative to the unmodified MSSQ:BTMSE (symbols connected with a line) films is shown as a function of relative indentation depth, h/t_f. A horizontal dotted line is shown to represent the value characteristic of bulk silicon ($D_{P\text{-}h} \approx 0.48$). The plots are divided into three main regions to illustrate (I) elastic-, (II) transition-, and (III) substrate-dominated regions.

These indentation traces showed increased hysteresis relative to the 0.3 mN indentation traces of Fig. 5. Similar to the trend observed for the 0.3 mN load, the relative displacement at peak load scaled with increased porosity (again, almost independent of porogen type). At this load, films made with the aromatic-core porogen exhibited a larger deviation in the indentation response from the unmodified MSSQ:BTMSE film relative to films made with the aliphatic-core porogen. For example, the lowest porosity film made from the aromatic-core porogen, $\phi = 0.06$, showed the same relative peak displacement as the highest porosity film, $\phi = 0.22$, made with the aliphatic-core porogen.

Discontinuities in the loading slope were apparent in the 10 mN indentation traces of all films, as shown in Fig. 6; similar characteristic features were correlated previously with film cracking.[28] Additional indentations were performed at a peak load slightly larger than the load at which the first discontinuity in loading slope was observed for each film. Figure 7a is a series of SEM images showing the residual damage from these indentations for unmodified MSSQ and the two lowest porosity MSSQ:BTMSE films. The peak indentation load, P_{max}, and film porosity, ϕ, are listed on each image. Figure 7b is the same set of images with the effective contact area at peak load drawn to scale over the image to highlight film cracking. (A detailed explanation of the determination of the contact area at peak load is described in a previous publication.[26])

In Fig. 7b it is clear that there is radial cracking extending substantially beyond the indentation contact area in the MSSQ film from a peak indentation load of $P_{max} = 3.5$ mN. In contrast, for peak indentation loads of 3 and 3.5 mN, porous MSSQ:BTMSE films showed very short radial cracks extending little beyond the contact area. For similar indentation loads, the crack lengths are clearly longer in the MSSQ film relative to the porous MSSQ:BTMSE films.

Figure 8 is a plot of dissipated energy ratio, $D_{P\text{-}h}$, as a function of relative displacement, h/t_f, for unmodified and porous MSSQ:BTMSE films. Films made with the aromatic-core porogen are shown in Fig. 8a, and films prepared with the aliphatic-core porogen are shown in Fig. 8b. Each symbol represents the mean and standard deviation of several indentations at a given peak load, summarizing the information from several $P\text{-}h$ traces, similar to those of Fig. 5 and 6, over the entire experimental indentation load range of 0.1-300 mN. The dissipated energy ratio for bulk silicon ($D_{P\text{-}h} = 0.48$) is shown as a horizontal dashed line.

The plots in Fig. 8 are divided into three regions highlighting elastic (I), transition (II), and substrate dominated (III) indentation behavior. The nearly elastic indentation responses observed for unmodified and low-porosity MSSQ:BTMSE films in Fig. 5 are reflected in the elastic region (I) of small energy dissipation in Fig. 8. Region II denotes a transition from small to large energy dissipation

Downloaded 20 Jul 2009 to 147.46.182.29. Redistribution subject to ECS license or copyright; see http://www.ecsdl.org/terms_use.jsp

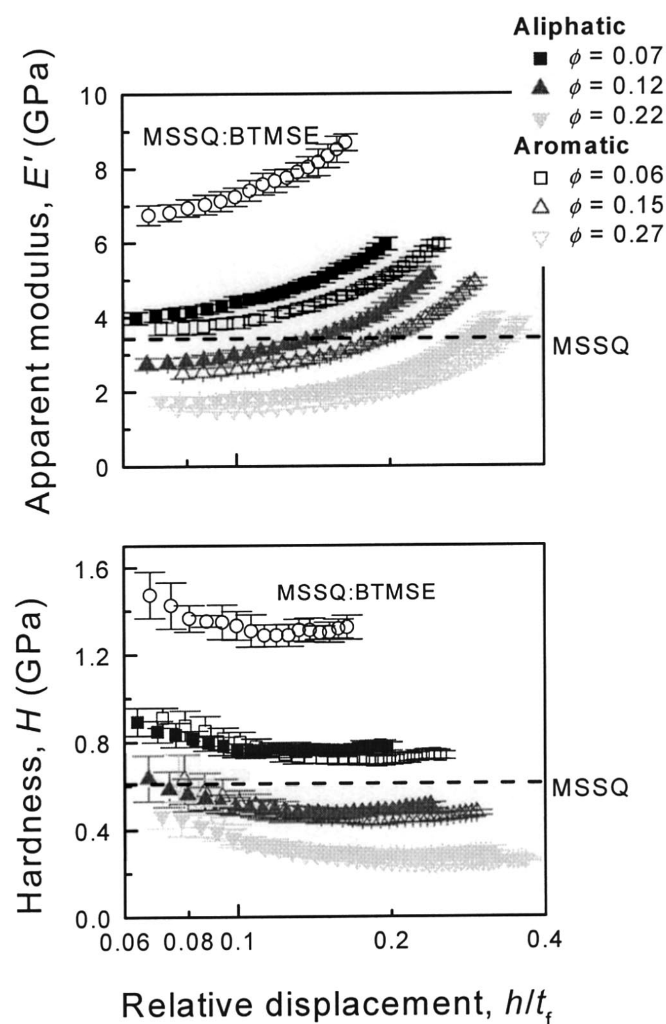

Figure 9. Apparent plane strain modulus, E', and hardness, H, of (○) unmodified and porous MSSQ:BTMSE films are shown as a function of relative displacement, (h/t_f), for a 0.3 mN peak load indentation. (■,▲,▼) Films made with the aliphatic core porogen and (□,△,▽) the aromatic core porogen are shown. Every symbol represents the average value calculated every 5 nm of displacement for several indentations, and error bars represent plus and minus one standard deviation. (— — —) Represents the values of MSSQ for comparison.

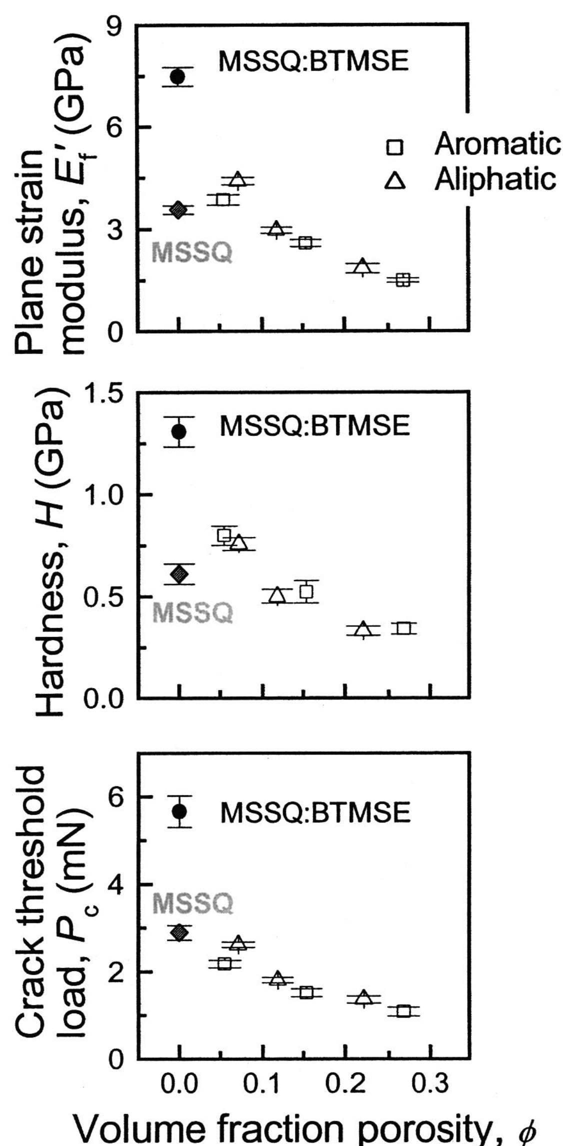

Figure 10. A plot summarizing E'_f, H, and P_c as a function of porosity, ϕ, for (●) unmodified and (□,△) porous MSSQ:BTMSE films. The values representative of (♦) unmodified MSSQ are shown for comparison. Symbols represent the average value of several indentations at $h/t_f = 0.1$, and error bars represent plus and minus one standard deviation.

as a function of increased h/t_f. This transition region reflects the increased degree of hysteresis observed with larger load indentations such as those shown in Fig. 6. Increased hysteresis is associated with the type of permanent deformation shown in the SEM images in Fig. 7. Dissipated energy reached a maximum value at the film-substrate interface $(h/t_f = 1)$, then decreased toward a value representative of the silicon substrate. This region of decreased energy dissipation reflects the dominating influence of the underlying silicon substrate in the indentation response.

Figure 9 is a plot of the apparent plane-strain modulus, E', and hardness, H, as a function of relative displacement, h/t_f, determined during a 0.3 mN peak indentation load. Each symbol represents the mean and standard deviation calculated every 5 nm of displacement. A dashed horizontal line indicates E' and H for the unmodified MSSQ film.[26] Values where the peak indentation depth was less than 50 nm are not shown as the indentation tip area function used in this analysis is not accurate at such shallow displacements. The slight increase in apparent modulus with increased relative indentation depth was attributed to increased substrate influence and was most dramatic for $h/t_f > 0.2$. Clearly the unmodified MSSQ:BTMSE film had the largest apparent modulus and modulus decreased with increased porosity (almost regardless of porogen type).

The unmodified MSSQ:BTMSE film also had the greatest hardness, and similar to the observed trend in apparent modulus, hardness decreased with increased porosity. While the modulus was more sensitive to slight differences in porosity, the hardness did not vary between films of slightly different porosities. In particular, the hardness of the lowest porosity films ($\phi = 0.06$ and 0.07) was the same (within experimental uncertainty) until a relative displacement of $h/t_f = 0.2$. Similarly, there was not a difference in the hardness of films with porosities 0.12 and 0.15 or films of porosity 0.22 and 0.27. Most importantly, the lowest porosity films, the films that had modulus values greater than MSSQ, also had hardness values greater than MSSQ.

To compare all the porous films with unmodified MSSQ and MSSQ:BTMSE films, average E' and H values at a relative displacement, $h/t_f = 0.1$ were determined. Figure 10 is a plot summarizing plane strain film modulus, E'_f, hardness, H, and crack thresh-

Downloaded 20 Jul 2009 to 147.46.182.29. Redistribution subject to ECS license or copyright; see http://www.ecsdl.org/terms_use.jsp

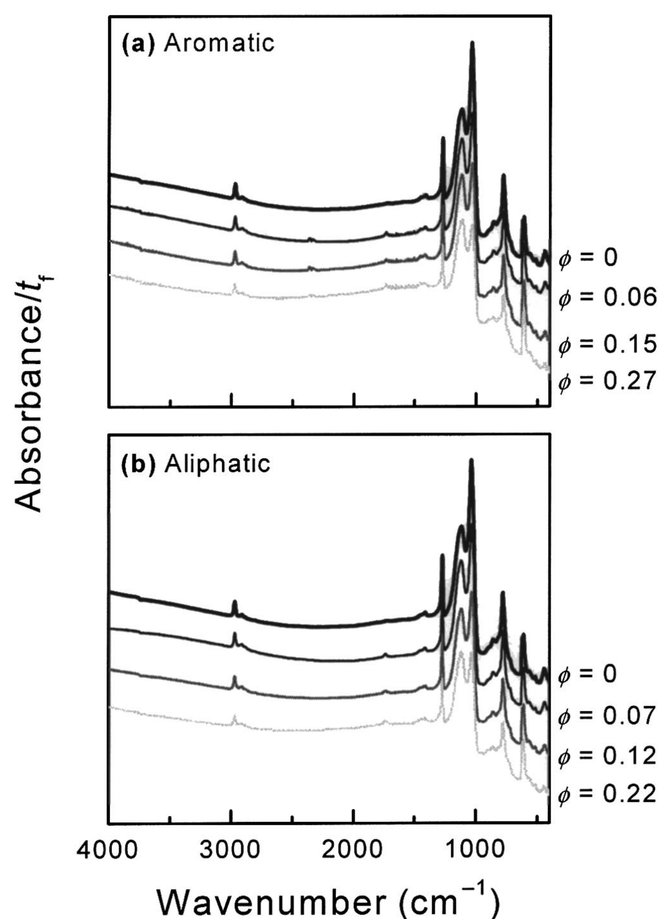

Figure 11. IR absorbance spectra of porous and unmodified MSSQ:BTMSE films are shown over a frequency range of 4000-400 cm^{-1}. Absorbance spectra were normalized by film thickness, t_f, and shifted on the abscissa for clarity. Spectra of films made with (a) aromatic and (b) aliphatic porogen relative to unmodified MSSQ:BTMSE film (bold line).

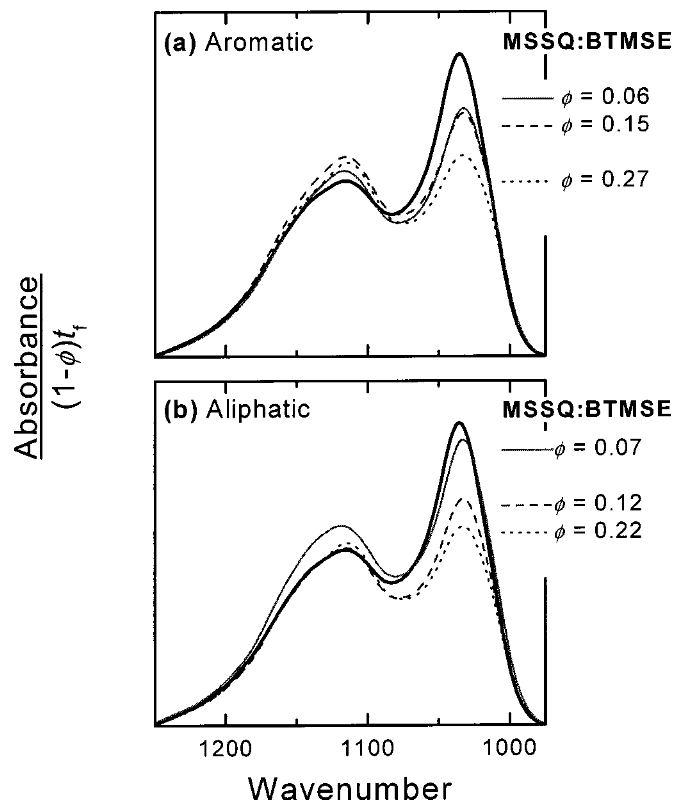

Figure 12. The O-Si-O stretching band is shown where spectra were baselined after normalizing by film thickness, t_f, and film density $(1-\phi)$. Spectra of porous films made with (a) aromatic-core porogen and (b) aliphatic-core porogen are shown relative to unmodified MSSQ:BTMSE film. Porosities are listed beside the spectra.

old load, P_c, with porosity, ϕ, for porous films relative to unmodified MSSQ and MSSQ:BTMSE films. Clearly the MSSQ:BTMSE copolymer film had the greatest E_f', H, and P_c of all films shown here. The decreased, E_f', H, and P_c with increased porosity of MSSQ:BTMSE films is also clearly shown. This plot, however, emphasizes the primary result, which is that the two lowest porosity films had greater modulus and hardness than the unmodified MSSQ film. This plot also illustrates the decreased modulus and hardness values that could be anticipated for porous MSSQ films. The threshold load for cracking, P_c, was smaller for all porous films relative to MSSQ.

IR spectra are shown in Fig. 11 for films made with the (a) aromatic-core porogen and (b) aliphatic-core porogen relative to the unmodified MSSQ:BTMSE film. In these plots, absorbance is normalized by film thickness, t_f, and shifted on the abscissa for clarity. The spectrum of MSSQ:BTMSE is shown as a bold line for comparison. The primary absorbance bands for all films include those associated with CH_3 stretching at 2900 cm^{-1}, CH_3 deformation at 1270 cm^{-1}, O-Si-O stretching from 1200 to 1000 cm^{-1}, and Si-C stretching and Si-CH_3 rocking at 780 cm^{-1}.[30-32]

The FTIR spectra appeared quite similar for all films except for the changes in relative peak intensity in the O-Si-O stretching band from 1200 to 1000 cm^{-1}. Changes in these normalized absorbance spectra reflect not only changes in bonding but also changes in film density due to porosity. To highlight the changes in the character of the spectra related only to changes in bonding (and not the number of absorbers), the normalized absorbance spectra in Fig. 11 were further normalized by film density $(1-\phi)$, then baseline corrected. Figure 12 shows the O-Si-O active region of the absorbance spectra normalized by film thickness and film density.

The specific interpretation of the O-Si-O active region can be found in a previous publication.[26] In Fig. 12, peak height at 1030 cm^{-1} associated with T-type (networked) species, $RSiO_{3/2}$, decreased with increased porosity, while the intensity of the peak at 1140 cm^{-1} associated with D-type species, R_2SiO, stayed the same or increased with increased porosity. An interpretation is that porogen domains hinder network formation of the matrix material, resulting in the decreased number of T species and increased number of D species. The relative peak heights of the O-Si-O networked and cage peaks have been previously correlated with porogen loading.[11] A similar trend was found for these films and the relative peak heights were evaluated by the peak height ratio, defined as the intensity of the peak at 1030 cm^{-1} normalized by the intensity of the peak at 1140 cm^{-1}.

Figure 13 is a plot of the peak height ratio as a function of porosity, ϕ. The relative amount of T- to D-type Si-O interaction was the greatest for the unmodified MSSQ:BTMSE film and decreased with increased porosity, highlighting the fact that the degree of networking in the films scaled with porosity. This suggests that porous MSSQ:BTMSE have smaller amounts of O-Si-O networking links than unmodified MSSQ:BTMSE films resulting from the formation of a porogen phase in the matrix that hinders matrix network formation during curing. Another interesting feature in this plot concerns the film with the largest ratio of networked O-Si-O to cage species of all porous films. This is the same film that was an exception to trends in both modulus and refractive index with porosity, as it had slightly greater porosity relative to the lowest porosity film

Downloaded 20 Jul 2009 to 147.46.182.29. Redistribution subject to ECS license or copyright; see http://www.ecsdl.org/terms_use.jsp

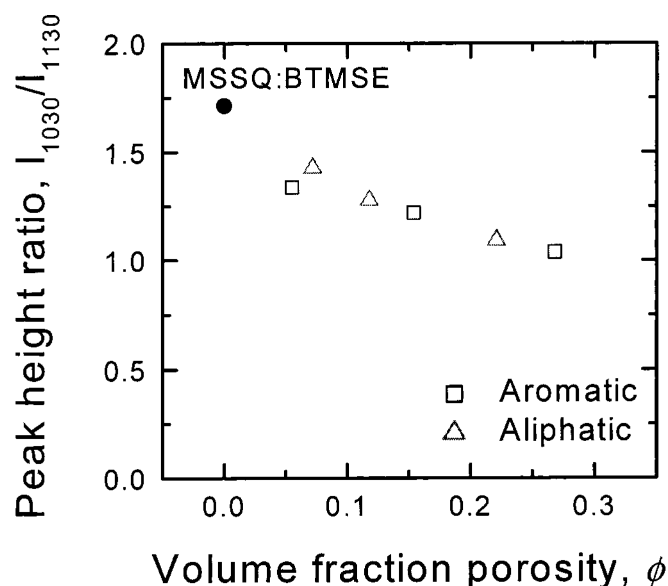

Figure 13. A plot of the ratio of peak intensity, *I*, of the two peaks in the O-Si-O band is shown as a function of porosity. This plot highlights the decreased number of networked species (T) relative to species with dangling -OH bonds (D) with increased porosity. The unmodified MSSQ:BTMSE film has the highest ratio of networked species and all porous films show smaller ratios.

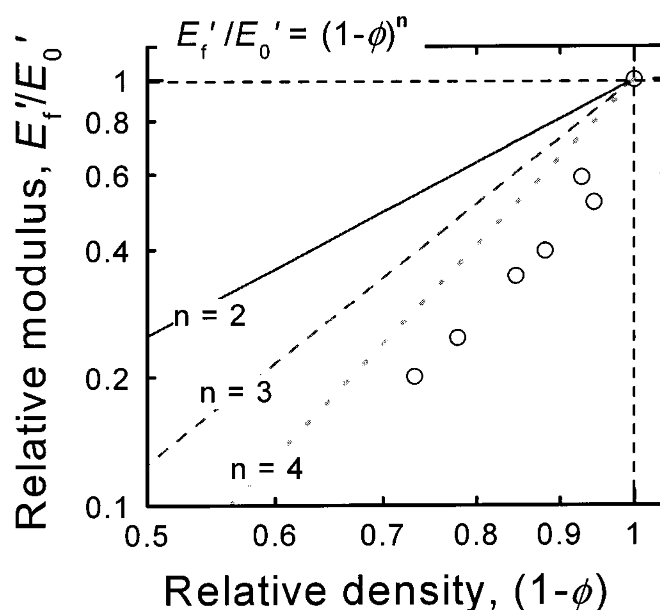

Figure 14. Plot of elastic modulus as a function of density for porous low-*k* materials; the affect of density of reduction on modulus is much greater than simple continuum models predict.

(ϕ = 0.06) and yet had a larger modulus, E_f', and larger crack threshold load, P_c.

Discussion

Incorporating porogen molecules modified the physical structure and mechanical properties of MSSQ:BTMSE films. Inferred volume fraction porosity, ϕ, increased with increased porogen loading, and the extent depended on porogen type. However, the individual contributions of porogen loading or type on pore size and pore density remain unclear. Pore size and pore density may have changed for a given porogen loading as a result of either the different core chemical structure or the different number of binding sites of the two porogen molecules. Positron annihilation lifetime spectroscopy (PALS) indicated that the average pore size increased from 1.9 (for ϕ = 0) to 2.2 (ϕ = 0.07) to 2.6 nm (ϕ = 0.12) for the film aliphatic-core porogen material, with larger pores in the aromatic-core material, consistent with the fracture surface observations in Fig. 3. However, the lack of strong distinction between the mechanical properties observed with the two different porogens suggests that differences in pore size and density are not sensed at the length scales of the measurements.

Film structure was also altered by porogen-matrix interaction, as shown by IR spectra. Figure 13 showed O-Si-O networking within the matrix material was disrupted by the addition of porogen. Relative to the unmodified MSSQ:BTMSE film the ratio of tri-coordinated (T) to bi-coordinated (D) O-Si-O species decreased as ϕ increased. The structural changes of decreased network formation in the matrix with increased porosity resulted in decreased modulus, E_f', hardness, *H*, of MSSQ:BTMSE films as shown in Fig. 10. Decreases in E_f' and *H* are consistent with the idea of pore collapse during indentation. Decreases in the cracking threshold load, P_c, however, are not so simply interpreted in terms of decreases in toughness, although both decreased network formation in the matrix and increased porosity would lead to decreases in toughness, *T*[28,33] (via a decrease in the number of bonds per unit area across a fracture plane and decreased modulus). Primary influences on cracking threshold include film stress, substrate constraint, and the nature of the defects and deformation generated during the indentation process, as well as the material toughness.[34] The decreases in P_c with ϕ observed here probably reflect decreased toughness in air with increasing porosity, but it is unclear that such a correlation would extend to the velocity of nonequilibrium extension of cracks in aqueous environments, as the latter phenomenon depends critically on the susceptilibity of film bonds to hydrolysis as well as film stress.[28,33]

The experimentally observed decrease in E_f' with ϕ may be compared to the relationship described by Gibson and Ashby,[35] which predicts that E' scales with relative density. The relationship between modulus and (open-cell) porosity predicted is

$$E_f' = C_1 E_0'(1-\phi)^2$$

where E_f' is the predicted modulus of the porous film, C_1 is a constant, E_0' is the modulus of the analogous solid film (taken as the base MSSQ:BTMSE case = 7.48 GPa), and $(1-\phi)$ is relative density.

Figure 14 is a plot of relative modulus, $E_f'/E_{(\phi=0)}'$, as a function of relative density where the experimentally measured values are shown (open circles) relative to the relationship predicted when $C_1 = 1$ (solid line). Experimentally, E_f' decreased more dramatically with decreased relative density than the predicted trend (changing the empirical amplitude term, C_1, also did not describe the experimental data). However, an exponent of the relative density term of approximately four does describe the experimental relationship (for $C_1 = 0.75$ the line passes through experimental data points). The experimentally measured decrease in E_f' with increased porosity is a stronger function of relative density than what was predicted. This is plausible because of the decreased networking of the matrix material with increased porosity (Fig. 13); this change in matrix material is unaccounted for by simple scaling relationships.

The primary result in the present study was the balance realized between the incorporation of porosity while maintaining mechanical properties for low-porosity MSSQ:BTMSE films with smaller refractive index, *n*, larger modulus, E_f', and hardness, *H*, and similar crack-threshold load, P_c, relative to the MSSQ film. This balance was achieved by physical modification of a base material with enhanced mechanical properties. Two chemical modifications, discussed in Part 1 of this series, were shown to improve mechanical properties of MSSQ films. First, a surface plasma treatment in-

Downloaded 20 Jul 2009 to 147.46.182.29. Redistribution subject to ECS license or copyright; see http://www.ecsdl.org/terms_use.jsp

creased the apparent surface E' and H of MSSQ films relative to the base MSSQ material. Second, the addition of a small amount of BTMSE increased E' and H to almost twice that of MSSQ films. This copolymer with enhanced mechanical properties served as the base material for the current study.

These studies in their entirety illustrate the effects of chemical and physical modifications of low-k films on mechanical properties, demonstrating the feasibility of creating porous low-k films while maintaining larger E' and H greater than that of analogous nonporous films.

Conclusions

1. Porous MSSQ:BTMSE films were prepared with two types of porogen, one with an aliphatic core and the other with an aromatic core.

2. Porogen loading changed the resulting film porosity to an extent dependent on the porogen type.

3. The formation of porogen domains hindered O-Si-O network formation of the MSSQ:BTMSE matrix.

4. Increased porosity as well as decreased network formation in the matrix resulted in decreased modulus, E_f', hardness, H, and cracking threshold load, P_c.

5. The lowest porosity films ($\phi \leq 0.07$) prepared with each porogen type had a smaller refractive index, n, and dielectric constant, k, and larger modulus, E_f', and hardness, H, than the MSSQ film.

6. Changing the matrix material from MSSQ to MSSQ:BTMSE copolymer resulted in the ability to introduce porosity and create a film with refractive index smaller than MSSQ along with modulus and hardness greater than MSSQ.

Acknowledgments

This work is supported by the Korean Collaborative Project for Excellence in Basic System IC Technology (System IC 2010: 98-B4-C0-00-01-00-02). Financial support from the Ministry of Science and Technology (MOST) and the Korean Ministry of Education through the National Research Laboratory Fund and the Brain Korea 21 Program, respectively, is also greatly acknowledged.

The University of Minnesota assisted in meeting the publication costs of this article.

References

1. *International Technology Roadmap for Semiconductors*, Semiconductor Industry Association, San Jose, CA (2002).
2. J. H. Golden, C. J. Hawker, and P. S. Ho, *Semicond. Int.,* **24**, 79 (2000).
3. C. Jin, J. D. Luttmer, D. M. Smith, and T. A. Ramos, *MRS Bull.,* **22**, 39 (1997).
4. T. G. Tsai, A. T. Cho, C. M. Yang, F. M. Pan, and K. J. Chao, *J. Electrochem. Soc.,* **149**, F116 (2002).
5. S. Baskaran, J. Liu, K. Domansky, N. Kohler, X. Li, C. Coyle, G. E. Fryxell, S. Thevuthasan, and R. E. Williford, *Adv. Mater. (Weinheim, Ger.),* **12**, 291 (2000).
6. J.-H. Kim, S.-B. Jung, H.-H. Park, and S.-H. Hyun, *Thin Solid Films,* **377-378**, 467 (2000).
7. B. Krause, G.-H. Koops, N. F. A. van der Vegt, M. Wessling, M. Wübbenhorst, and J. van Turnhout, *Adv. Mater. (Weinheim, Ger.),* **14**, 1041 (2002).
8. Y. F. Chow, T. H. Foo, L. Shen, J. S. Pan, A. Y. Du, Z. X. Xing, Y. J. Yuan, C. Y. Li, R. Kumar, and P. D. Foo, *Mater. Res. Soc. Symp. Proc.,* **716**, B12.2.1 (2002).
9. J. L. Hedrick, T. P. Russell, M. Sanchez, R. DiPietro, S. Swanson, D. Mecerreyes, and R. Jerome, *Macromolecules,* **29**, 3642 (1996).
10. C. V. Nguyen, K. R. Carter, C. J. Hawker, J. L. Hedrick, R. L. Jaffe, R. D. Miller, J. F. Remenar, H. W. Rhee, P. M. Rice, M. F. Toney, M. Trollsas, and D. Y. Yoon, *Chem. Mater.,* **11**, 3080 (1999).
11. Q. R. Huang, W. Volksen, E. Huang, M. Toney, C. W. Frank, and R. D. Miller, *Chem. Mater.,* **14**, 3676 (2002).
12. S. Yang, P. A. Mirau, C.-S. Pai, O. Nalamasu, E. Reichmanis, J. C. Pai, Y. S. Obeng, J. Seputro, E. K. Lin, H.-J. Lee, J. Sun, and D. W. Gidley, *Chem. Mater.,* **14**, 369 (2002).
13. A. M. Padovani, L. Rhodes, S. A. B. Allen, and P. A. Kohl, *J. Electrochem. Soc.,* **149**, F161 (2002).
14. A. M. Padovani, L. Riester, L. Rhodes, S. A. B. Allen, and P. A. Kohl, *J. Electrochem. Soc.,* **149**, F171 (2002).
15. B. Zhong, H. Meynen, F. Iocopi, K. Weidner, S. Mailhouitre, E. Moyer, C. Bargeron, P. Schalk, A. Peck, M. Van Hove, and K. Maex, *Mater. Res. Soc. Symp. Proc.,* **716**, B12.4.1 (2002).
16. H.-J. Lee, E. K. Lin, W. Wang, W.-L. Wu, W. Chen, and T. A. Deis, *Mater. Res. Soc. Symp. Proc.,* **714**, L7.11.1 (2001).
17. C. J. Hawker, J. L. Hedrick, R. D. Miller, and W. Volksen, *MRS Bull.,* **25**, 54 (2000).
18. M. E. Thomas, N. Iwamoto, D. Smith, and S. Wallace, *Semicond. Int.,* **25**, 105 (2002).
19. G. W. Ray, *Mater. Res. Soc. Symp. Proc.,* **511**, 199 (1998).
20. R. Bajaj, A. Zutshi, R. Surana, M. Naik, and T. Pan, *MRS Bull.,* **27**, 776 (2002).
21. W.-C. Chen and C.-T. Yen, *J. Vac. Sci. Technol. B,* **18**, 201 (2000).
22. W.-C. Chen, S.-C. Lin, B.-T. Dai, and M.-S. Tsai, *J. Electrochem. Soc.,* **146**, 3004 (1999).
23. V. P. Atluri, R. V. Mahajan, P. R. Patel, D. Mallik, J. Tang, V. S. Wakharkar, G. M. Chrysler, C.-P. Chiu, G. N. Choksi, and R. S. Viswanath, *MRS Bull.,* **28**, 21 (2003).
24. S. M. Kim, D. Y. Yoon, C. V. Nguyen, J. Han, and R. L. Jaffe, *Mater. Res. Soc. Symp. Proc.,* **511**, 39 (1998).
25. R. F. Cook, *Mater. Res. Soc. Symp. Proc.,* **576**, 301 (1999).
26. S. Kim, Y. Toivola, R. F. Cook, K. Char, and D. Y. Yoon, *J. Electrochem. Soc.*, **151**, F37 (2003).
27. J.-K. Lee, K. Char, H. W. Rhee, H.-W. Ro, D. Y. Yoo, and D. Y. Yoon, *Polymer,* **42**, 9085 (2001).
28. Y. Toivola, J. Thurn, and R. F. Cook, *J. Electrochem. Soc.,* **149**, F9 (2002).
29. W. C. Oliver and G. M. Pharr, *J. Mater. Res.,* **7**, 1564 (1992).
30. C. Y. Wang, Z. X. Shen, and J. Z. Zheng, *Appl. Spectrosc.,* **54**, 209 (2000).
31. C. Y. Wang, Z. X. Shen, and J. Z. Zheng, *Appl. Spectrosc.,* **55**, 1347 (2001).
32. G. Socrates, *Infrared and Raman Group Characteristic Frequencies: Tables and Charts*, John Wiley & Sons, Inc., New York (2001).
33. R. F. Cook and E. G. Liniger, *J. Electrochem. Soc.,* **146**, 4439 (1999).
34. D. J. Morris and R. F. Cook, *Mater. Res. Soc. Symp. Proc.,* **766**, E9.3.1 (2003).
35. L. J. Gibson and M. F. Ashby, *Cellular Solids: Structure and Properties*, 2nd ed., p. 186, Cambridge University Press, Cambridge, MA (1997).

Downloaded 20 Jul 2009 to 147.46.182.29. Redistribution subject to ECS license or copyright; see http://www.ecsdl.org/terms_use.jsp